Inner energy relaxation and growth of nanosize particles

M. Bredice,[1,*] M. G. Rozman,[1] J. Smucker,[1] E. Farmer,[1] R. Côté,[2] and V. Kharchenko[1,3]
[1]*Department of Physics, University of Connecticut, Storrs, Connecticut 06269, USA*
[2]*UMass-Boston, Department of Physics, Boston, Massachusetts 02125, USA*
[3]*ITAMP, Center for Astrophysics | Harvard & Smithsonian, Cambridge, Massachusetts 02138, USA*

(Received 23 March 2023; accepted 14 August 2023; published 11 September 2023)

In this study, molecular-dynamics simulations were conducted to investigate the relaxation of the internal energy in nanosized particles and its impact on the nucleation of atomic clusters. Accurate binary potentials were utilized to analyze the growth and collisional relaxation of the internal energy of Ar_nH^+ clusters in a metastable Ar gas. The results revealed that small nanoclusters are formed in highly excited rotational-vibrational states and that the relaxation of internal energy and growth of these nascent clusters are concurrent processes with a strong mutual influence. Under nonequilibrium growth conditions, the relaxation of internal energy can delay the cluster growth process. The rates of cluster growth and internal energy relaxation were found to be influenced by the energy-transfer collisions between cluster particles and free Ar atoms of the bath gas. Furthermore, the nonequilibrium growth and internal energy relaxation of small nanoclusters were found to depend on the structure of the cluster's atomic shells. An ensemble of molecular-dynamics simulations was conducted to investigate the growth and time evolution of the kinetic and total energies of Ar_nH^+ clusters with specified $n \leqslant 11$, and the results were explained by collisional relaxation processes described by the Boltzmann equation. Finally, the general relationship between the rates of internal energy relaxation and nonequilibrium growth of nanoparticles is discussed.

DOI: 10.1103/PhysRevA.108.032812

I. INTRODUCTION

The nucleation of a new phase from a gas or liquid has been studied for many years across a range of fields, including physics, chemistry, astrophysics, and planetary science. For example, the analysis of the formation of nanosize ice and dust particles is critical for determining their spectral properties in the upper atmospheres of exoplanets [1–6] or in circumstellar disks [7–9]. Classical nucleation theory [10–13] has been relatively successful in analyzing nucleation processes in mesoscopic and large-size systems under thermal equilibrium conditions but is not suitable for describing the nonequilibrium nucleation of nanoparticles and clusters. Theoretical modeling of the onset of the nucleation process is challenging when nanoparticles grow under local nonequilibrium and nonhomogeneous conditions. Detailed knowledge of the relaxation processes in nanoscale objects is needed to understand how nanoparticles evolve toward their equilibrium state. The initial stages of nucleation must be considered as a local exothermic process due to the significant release of kinetic energy during the growth of a new phase. As an illustration of this general phenomenon, we consider the nucleation of nanosize atomic clusters in $Ar_nH^+ + Ar \rightarrow Ar_{n+1}H^{+*}$ transitions. As a result, small nanoparticles are formed in highly excited rotational-vibrational states, and their internal energy relaxation occurs alongside cluster growth. The processes of cluster energy relaxation and nucleation strongly influence each other, creating a complex picture of nanoparticle growth. Accurate knowledge of interparticle interactions is necessary to describe possible relaxation mechanisms and their effects on the rate of formation of the new phase, the cluster particles.

Previous investigations of atomic clusters have demonstrated that molecular-dynamics (MD) simulations with accurate potentials of interparticle interactions can describe both nonequilibrium and equilibrium processes of the nucleation of nanosize particles. In the past, there has been a significant amount of research utilizing MD methods to study the nucleation of various clusters. For instance, some investigations have focused on pure Ar clusters; specifically on their associated structure [14], phase transitions [15,16], and kinetics of their nucleation [17,18]. In addition, there have been recent investigations of the phase transitions of protonated Ar clusters using classical MD simulations [19]. Moreover, there has been a large focus on the nucleation of clusters composed of molecules commonly found in atmospheres, including the growth of water and ice clusters [20–23], and the study of the structure of aerosol nanoparticles [24]. In the past, there also have been some theoretical analyses of small Ar_nH^+ and Lennard-Jones (LJ) clusters. The focus of those investigations was on the respective ground-state structures and explanation of "magic numbers" associated with experimental data [25–29]. There also is a large amount of laboratory research using supersonic-beam experiments involving different species of nanoparticle-sized clusters; where those experiments investigate the growth and abundance of nanoparticle-sized clusters with different numbers of atoms [25,30–40]. However, these investigations did not consider that small nascent clusters are formed in highly excited states

*mitchell.bredice@uconn.edu

and this establishes the relationship between nonequilibrium cluster growth and its internal energy relaxation.

In this study, MD simulations of the growth of Ar_nH^+ clusters initiated in a metastable Ar gas by H^+ ions were performed. The results showed that nanoparticles of noble gas atoms, seeded by an ion, are initially formed in highly excited rotational and vibrational states. The energy of the cluster, both the center of mass and internal components, undergoes relaxation through collisions with atoms of the ambient Ar gas. The relaxation of internal energy significantly influences the growth of nanosize clusters. This type of effect has previously been observed in the nucleation of metallic nanoparticles [41].

The growth of clusters in a bath gas has a large number of relaxation pathways, with energy relaxation being a fundamental one [42,43]. The mechanisms and rates of energy relaxation for the cluster's translational or internal degrees of freedom can be quite different. In a relatively dense ambient gas, the initial translational energy of nascent clusters is efficiently dissipated through multiple collisions with free atoms. The relaxation of the internal kinetic energy of growing clusters can include several pathways, such as the transfer of a fraction of the internal energy in atom-cluster cooling collisions or detachment processes; in which, the energetic atoms leave the cluster and significantly reduce the cluster's internal energy. For example, the decay of a metastable Ar_nH^{+*} cluster, which was formed in highly excited rotational-vibrational states, can significantly reduce its internal energy through the auto-detachment process $Ar_nH^{+*} \rightarrow Ar_{n-1}H^+ + Ar + \Delta\epsilon$, where $\Delta\epsilon$ is the kinetic energy of the ejected Ar atom.

The relaxation of hot particles due to energy transfer collisions with a bath gas has been extensively studied for atomic and molecular species [44–48]. The large number of inelastic-collision channels, which lead to excitation of the cluster's internal degrees of freedom, complicate the theoretical description of the energy relaxation of small clusters. As a result, some studies have focused on the postcollision relaxation of clusters that are excited by a single collision [49,50]. In dilute environments, radiation cooling and heating mechanisms can become important but are neglected in our investigations because collisional relaxation occurs much faster.

The fundamental problem in the physics of nanoparticle nucleation is to establish general rules that govern the kinetics of cluster formation and growth under nonequilibrium conditions. The rates of relaxation of inner cluster energy and cluster growth influence each other and both strongly depend on the local parameters of the surrounding gas. Detailed analysis of the rates of atomic sticking and detachment processes in collisions with nanosize clusters could provide insight into predicting the cluster size-distribution under nonequilibrium and equilibrium conditions. In high-density environments (solid or liquid), the energy relaxation may be dominated by many-body or bulk effects. However, in the gas environment, the processes of relaxation of the internal cluster energy are relatively simple due to the majority of collisions being single atom-cluster collisions. These collisions simultaneously regulate the rates of cluster cooling and growth.

The current study aims to investigate nucleation under local nonequilibrium conditions, the initial growth of nascent clusters during this nonequilibrium nucleation, and the relaxation of kinetic and potential energies of nascent clusters. To our knowledge, there has not been a comprehensive study surrounding these topics in the literature.

II. SIMULATION DETAILS

In this study, we used molecular-dynamics (MD) simulations to investigate how the internal energy relaxation of nascent nanoclusters affects the nucleation process. We performed the simulations using the Large Atomic/Molecular Massively Parallel Simulator (LAMMPS) [51]. All simulations are performed with periodic boundary conditions along all spatial dimensions. The binary Ar-Ar and Ar-H^+ interactions are described in detail in Ref. [19]. Each simulation began with the random generation of coordinates of 1000 Ar atoms and a single H^+ ion, with a minimum distance of 3 Å between each particle. The velocities of the Ar atoms were initialized using the LAMMPS "create velocity" function, while the initial H^+ velocity for convenience was set to zero. In our simulations, the initial speed distribution of the Ar atoms had a Gaussian shape, with its average corresponding to the speed of the average kinetic energy of the desired temperature. These initial conditions are analogous to a sudden quench of the Ar gas to a metastable quasi-equilibrium state followed by the ionization of a hydrogen atom. As in our simulations, we found that the system's speed distribution quickly becomes Maxwellian-like on timescales faster than the cluster nucleation. Therefore the cluster will form locally around a quasi-equilibrium metastable gas. Moreover, due to the large release of energy during nucleation (to be described in Sec. III), the local environment of the cluster will determine the growth, not the overall system's distribution function. Therefore the nonequilibrium growth should not be sensitive to sensible initial conditions. We performed simulations at two temperatures, below and above the Ar boiling point, 40 and 90 K, respectively. In all of our simulations, the Ar density was 10^{20} cm^{-3}. These temperatures and density of the Ar buffer gas were chosen so that the Ar_nH^+ clusters can grow to sizes $n \approx 10$ within a few nanoseconds and that allows a lower computational time for each individual simulation. We ran 500 simulations with unique initial conditions for each temperature, with a total simulation time of 2.5 ns. In our previous work, we found that small clusters grew relatively quickly, in ≈2–5 ns, at a temperature of 90 K [52]. The rate of nucleation of nanoclusters was significantly increased at lower temperatures, such as 40 K.

All simulations were performed with a time step of 1 fs, using the canonical (NVT) ensemble with a Nose-Hoover thermostat and a temperature damping timescale of 100 fs. The MD trajectories were recorded at 1 ps intervals. This arrangement of simulations provides the necessary data for the analysis of the dynamics of the internal degrees of freedom and the motion of the center of mass for each cluster. To analyze the cluster parameters, we used the DBSCAN algorithm implemented in the Clustering.jl package of the Julia programming language. A more detailed discussion of the cluster definition and DBSCAN parameters can be found in Ref. [52]. However, for each cluster, its total energy is calculated to ensure it is negative to indicate a true bound cluster.

Our choice of a Nose-Hoover thermostat may provide a nonphysical mechanism to exchange energy with the cluster particles. However, in our simulations, it has minimal impact on the relaxation of the cluster's kinetic energy, which is efficiently regulated due to collisions with the Ar bath gas. The thermostat mostly affects Ar atoms in the free gas, supporting their temperature (majority of overall system energy) while minimally extracting the cluster's energy. This is due to the much larger fraction of free Ar atoms compared with the cluster's atoms. We have checked that this is the case by performing a smaller set of simulations with thermostat damping times of 1000 and 10 000 fs, which are weaker or slower thermostat couplings. We found our choice of 100 fs for the damping time had no significant impact compared with the weaker thermostats; therefore we can ignore the thermostat for the purposes of our investigation. Moreover, this effect was also demonstrated in the case of the nucleation of pure Ar clusters [53], where different types of thermostats investigated, including Nose-Hoover, had no impact on the cluster temperature (kinetic energy). However, we do note that a choice of smaller damping time (strong or faster couplings) could introduce significant thermostat effects; or if many ions are present then thermostat effects would need to be sufficiently checked due to the much larger release of potential energy.

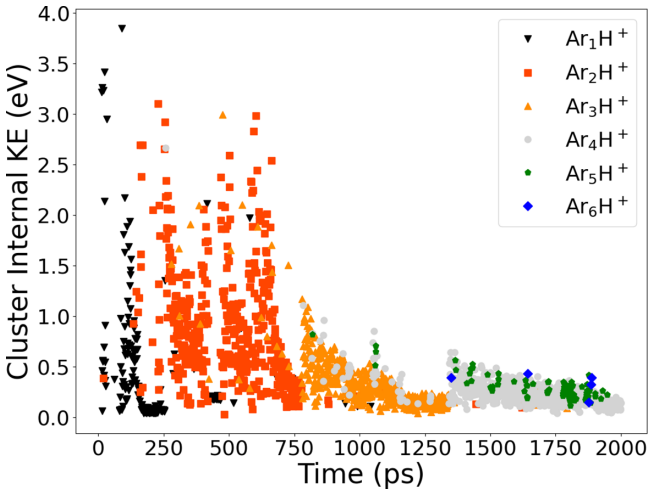

FIG. 1. Shown is the internal kinetic energy for an $Ar_{n(t)}H^+$ cluster ($n \leqslant 6$), from a single MD simulation trajectory, where the simulation was performed at 90 K. Different marker types and colors indicate changes in cluster size. It is apparent in the first $n \rightarrow n+1$ size transitions that the nascent clusters have a large amount of internal energy, which decreases before subsequent n growth. The $n = 4$ clusters (gray points) exhibit stability by remaining present at long timescales.

III. FORMATION OF NASCENT Ar_nH^+ CLUSTERS

The current MD simulations have three specific goals. The first is to show that small Ar_nH^+ clusters are formed in highly excited rotational-vibrational states, or in highly excited geometrical configurations. The second goal is to determine the relationship between the rate of cluster growth and the rate of internal energy relaxation. The third is to establish how the cooling and growth rates of small nanoclusters depend on the parameters of the ambient gas. The simulations carried out in this work can clarify the dynamics of nonequilibrium cooling of internal degrees of freedom in clusters of different sizes. At low densities of the ambient gas, the cooling of small nanoclusters may be a "bottleneck" in the entire nucleation process and must be "stepped through" before a cluster can grow.

To simulate the growth of independent clusters, only one H^+ ion is present in the simulation box, allowing for the formation and tracking of a single $Ar_{n(t)}H^+$ cluster in the simulation time from each MD trajectory. This allows one to investigate the evolution of a single independent cluster and to avoid the additional complications that arise due to the simultaneous nucleation of many clusters around individual H^+ ions; where competition between the growth of different clusters leads to the coalescence regime [13,52].

The cluster's internal kinetic energy represents the sum of the kinetic energy of all the cluster's particles with the cluster's center-of-mass (CM) energy removed. The total internal energy of the cluster in the CM frame is the sum of the internal kinetic energy of all cluster's atoms and the potential energy of their interaction. The data on the time-dependent relaxation of the Ar_nH^+ internal energies, i.e., specifically the kinetic, potential, and total energies of the atoms inside the cluster, have been recorded and analyzed. The relaxation of the cluster's potential energy, which is an essential part of the internal energy, reflects the continuous transformation of the cluster's geometrical configuration through the entire cooling process. To establish a time-dependent picture of the relaxation of the internal kinetic and total energies of Ar_nH^+ clusters, these energies have been computed every ps that a cluster exists and tracked through time along with the time-dependent cluster size $n = n(t)$. To illustrate the tracking procedure, the evolution of the cluster internal kinetic energy, denoted as ε_k, for an Ar_nH^+ cluster in a single simulation trajectory is shown in Fig. 1.

The results of a single H^+ simulation depicted in Fig. 1 also illustrate the time-evolution of the size $n(t)$ of $Ar_{n(t)}H^+$ clusters (via marker color and shape). The dynamics of cluster growth include both processes, the size increases $n \rightarrow n+1$ and decays $n \rightarrow n-1$, which occur with different probabilities during the nonequilibrium nucleation of small clusters. The probability of $n \rightarrow n+1$ transitions, i.e., the probability of the sticking collisions between clusters and free Ar atoms surpasses the decay probability during the nonequilibrium stage of nucleation. The probabilities of both these processes became equal when the system has reached equilibrium between the gas and cluster phase.

There are several noteworthy observations that can be made from analyzing the relaxation of cluster energies. First, we notice the remarkable stability of the Ar_4H^+ cluster, which has the first closed shell. This cluster generally does not demonstrate $n \rightarrow n-1$ transitions, as it is extremely stable with deep binding energies of the cluster Ar atoms [52]. Moreover, the Ar_4H^+ cluster exists in the broad time-domain that overlaps significantly with time-regions that belong to other clusters. It means that, under nonequilibrium conditions, any decay of larger clusters, such as Ar_5H^+ or Ar_6H^+, could end up returning with a high probability to the stable configuration of Ar_4H^+. Second, the growth of small clusters through the collision reaction $Ar_{n-1}H^+ + Ar \rightarrow Ar_nH^{+*}$, leads to a

sharp increase in the cluster's internal energy. The average value of the release of internal kinetic energy approximately corresponds to the absolute value of the chemical potential of Ar atoms in the Ar_nH^+ cluster [52]. For small-sized clusters, which can be considered as molecular ions Ar_nH^+, the $n \to n+1$ growth leads to multiple excitations of vibrational and rotational modes. Although the growth of small-n clusters causes a significant excitation of the cluster's internal degrees of freedom, the magnitude of this excitation decreases with cluster size n [52]. The fact that the magnitude of excitation decreases with cluster size n also implies that the cluster becomes progressively easier to grow from an energetic standpoint, as less internal energy would need to be cooled before subsequent growth. Additionally, the internal kinetic energy released in $n \to n+1$ transitions is much larger than k_BT, the scale of thermal energy limiting the cluster growth under equilibrium conditions. This means that the excited state of nascent clusters can persist for a relatively long time, which is required for the cooling of nascent clusters. This time depends on the size of the cluster and the efficiency of cooling collisions between Ar_nH^{+*} and cold atoms of the ambient Ar gas.

Another notable observation is that the $Ar_{n-1}H^+ + Ar \to Ar_nH^{+*}$ sticking collisions can lead to the formation of long-living metastable clusters. They can dissociate in spontaneous $n \to n-1$ transitions or could be a channel of fast cooling via quenching collisions $Ar_nH^{+*} + Ar \to Ar_nH^+ + Ar^*$. It appears that the time needed for nascent clusters to relax from the initial rotational-vibrational excited state (i.e., the lifetime of the excited Ar_nH^{+*} clusters) plays a role in mediating the growth of Ar_nH^+. For specific densities and temperatures of the atomic gas, the relaxation of the internal energy acts as a "bottleneck" in the growth process.[1]

Highly excited states of cluster particles can be successfully described by the methods of classical molecular dynamics. Despite their small size, Ar_nH^+ clusters are known to have a significant number of soft-vibrational modes [26,28,54], which provide a large density of excited states and contribute to the ongoing semiclassical dynamics of the internal energy relaxation. As shown in Fig. 1, the initial formation of small clusters is accompanied by large energy excitation of the internal degrees of freedom, which justifies the use of the classical MD simulations of the nucleation process.

IV. ENSEMBLE AVERAGE METHODS

To investigate the stochastic processes that govern the energy relaxation of a cluster, we generated an ensemble of 500 MD trajectories. These trajectories provide insight into the average behavior of the system and allow us to examine the nucleation of independent clusters induced by an individual H^+ ion. To further understand the time-dependent kinetics of Ar_nH^+ nucleation, we calculated ensemble-average quantities for clusters containing the same number of Ar atoms n, accounting for the time since the creation of Ar_nH^+ clusters. The generated MD trajectories represent an ensemble of independently growing Ar_nH^+ clusters.

In the present study, several computational steps were implemented to analyze the data obtained from MD simulations of the nucleation of Ar_nH^+ clusters. Specifically, for each MD trajectory, the data on the formation and evolution of the clusters was analyzed, and any outlying data was removed using a simple clustering algorithm based on temporal information. The purpose of this procedure was to identify the average time interval during which the cluster size remained stable at n rather than being temporarily changed due to close encounters between the Ar_nH^+ cluster and free Ar atoms. These encounters can lead to a temporary "fictitious growth" from n to $n+1$ when using the DBSCAN algorithm on LAMMPS trajectories to classify clusters based on the geometric proximity of atoms. However, this growth is typically short-lived and returns to a stable size within 1–2 ps. We effectively employed the time-filtering procedure that removed the majority of these temporary "fictitious growth" events from the ensemble data.

Moreover, due to size fluctuations, it is possible that a cluster could return to its original size after growing, e.g., $n = 3 \to 4$ to $n = 4 \to 3$, by ejecting an atom after some short time that is not excluded via the simple clustering algorithm. In the event of this, the "new" $n = 3$ cluster is treated as a continuation of when it originally grew to $n = 3$, albeit with a gap in the time since it formed. However, its energy after returning to its original size would still be consistent with energy relaxation as it will release kinetic energy by ejecting an atom. Therefore our approach is self-consistent without introducing new clusters to the ensemble, but only continuing the dynamics from the original time it formed. However, in the data provided from our simulations, this process was minimally observed.

To study the time-dependent cooling process in the ensemble of clusters of a specific size n, the ensemble data on nascent Ar_nH^+ clusters were scaled to artificially start at $t = 0$. This new effective time of cluster creation at $t = 0$ coincides with the first time step at which the cluster is observed to be the desired size n. This scaling is necessary because the moment when an individual Ar_nH^+ cluster becomes the desired size is random in absolute time. However, by scaling all clusters of size n to start at a common $t = 0$, their energy relaxation dynamics can be compared and $t = 0$ can be interpreted as the "time since formation," t_f.

After the scaling described above, all of the cluster data for the specific size n have a common time domain. This allows one to calculate the ensemble average values at every time since formation with the adopted time step of 1 ps. To calculate the ensemble average of various cluster parameters such as the cluster internal energy, center-of-mass energy, internal kinetic energy, potential energy, and the energy distribution functions for the cluster's Ar and H^+ particles, these quantities are binned to create time-dependent empirical probability distributions. These distributions are used to calculate the appropriate time-dependent average values at every subsequent point in time after $t = 0$. The empirical probability distribution must be rebuilt at every time step after the time since formation due to the ongoing growth and decay of the

[1]There is an analogy between the cluster nucleation and the processes of electron-highly charged ion recombination in the plasma physics, which involves the capture of electrons into highly excited Rydberg states and subsequent relaxation of the ion internal energy [13].

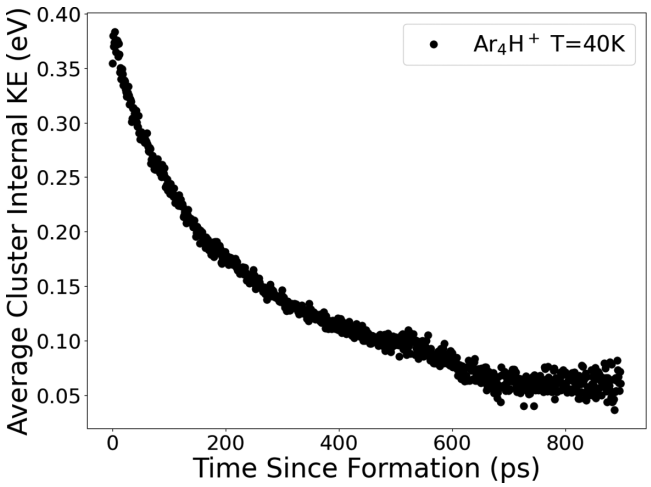

FIG. 2. The ensemble average of the internal kinetic energy $\overline{\varepsilon_k}$ is shown for Ar_4H^+ clusters at a temperature of 40 K. The average is calculated from a series of simulations and shows a smooth decrease in internal energy with small fluctuation.

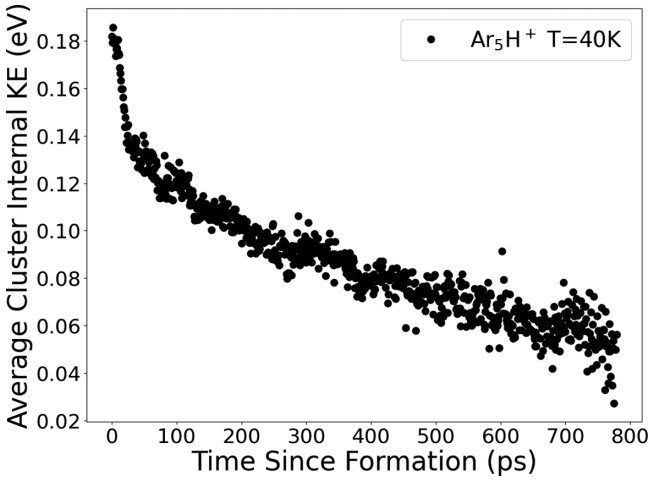

FIG. 4. The ensemble average of the internal kinetic energy $\overline{\varepsilon_k}$ is shown for Ar_5H^+ at a temperature $T = 40$ K. This average is calculated from a series of simulations and shows a sharp energy relaxation within the first 100 ps, followed by a smooth behavior thereafter.

cluster size n. The time evolution of the number of clusters of a given size n will be discussed in Sec. VI.

V. ENERGY RELAXATION IN THE ENSEMBLE

The formation of Ar_nH^+ clusters is initially characterized by nonequilibrium configurations, which can be alternatively represented as a superposition of highly excited rotational-vibrational states. Through simulations, we have identified the time-dependent kinetics of cluster growth and observed the mechanisms by which the internal kinetic energy of the cluster relaxes. The time-dependent picture of the internal energy relaxation in the ensemble of nascent Ar_nH^{+*} clusters is shown through the ensemble average of the internal kinetic, $\overline{\varepsilon_k}$ in Figs. 2 and 4; and total energies, $\overline{\varepsilon_{\text{tot}}}$ in Figs. 3 and 5, for clusters with $n = 4$ and 5 at $T = 40$ K. In the time dependence of the internal kinetic energies $\overline{\varepsilon_k}$ of clusters with $n = 4$ and 5, shown in Figs. 2 and 4, we see some notable features. One is that the relaxation is generally smooth, with relatively small fluctuations. The relaxation of the total energy $\overline{\varepsilon_{\text{tot}}}$ (Figs. 3 and 5) is even smoother with smaller fluctuations despite it including the simultaneous fluctuating kinetic and potential (configuration) energies. In our simulations, these clusters never reach thermal equilibrium before their subsequent growth. Although their internal energy relaxes during their entire lifetime, the cluster kinetic energy is still larger

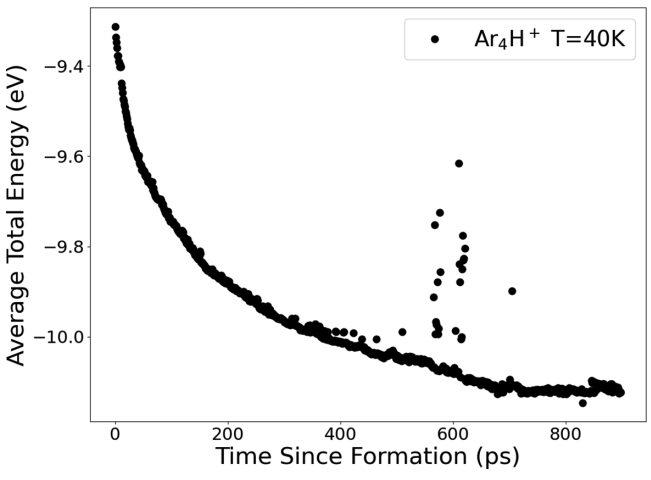

FIG. 3. The ensemble average of the total energy of cluster particles, $\overline{\varepsilon_{\text{tot}}}$, is shown for Ar_4H^+ clusters at a temperature $T = 40$ K. This average is calculated from a series of simulations and shows a smooth behavior except for isolated fluctuation near 600 ps.

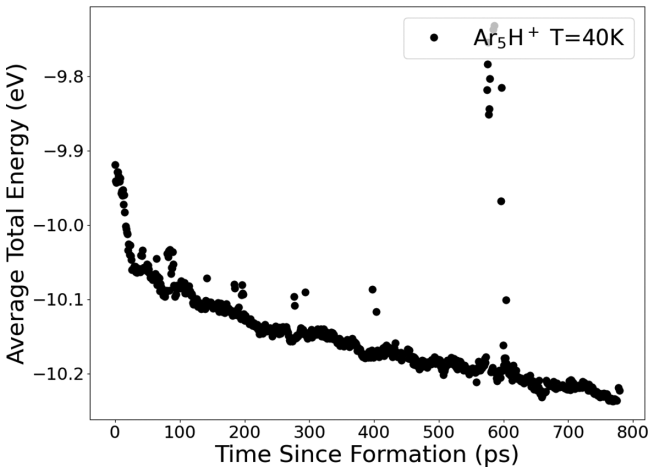

FIG. 5. The ensemble average of the total energy of cluster particles, $\overline{\varepsilon_{\text{tot}}}$, is shown for Ar_5H^+ clusters at a temperature $T = 40$ K. The average is based on the results of multiple simulations. A significant increase in the total internal energy, shown as a spike around $t = 600$ ps, is observed. This spike is only ≈4% different relative to the surrounding curve. This is attributed to a small group (approximately 20%) of clusters, with initial configurations very far from the ground-state configuration providing the cluster's minimal energy. These clusters relax slowly and can contribute to the deviation from the average total energy.

than the thermal equilibrium energy of $\frac{3}{2}(n-1)k_BT$ ($T = 40$ K) corresponding to the internal motion of the atoms. This means that these small clusters have been produced stably and disappeared from their Ar_nH^+ ensemble due to the size growth or evaporation before reaching thermal equilibrium.

One of the objectives of this study is to investigate the relationship between the average kinetic energy of cluster particles per internal degree of freedom $\overline{\epsilon_n}$ and the kinetic energy of their center of mass (CM). For all values of n examined, the CM kinetic energy was found to be significantly lower compared with $\overline{\epsilon_n}$. However, as the internal degrees of freedom of the cluster approached thermalization, both the CM kinetic energy and $\overline{\epsilon_n}$ became comparable to the thermal energy $\frac{3}{2}k_BT$. Our results suggest that studying the relaxation of internal energy is an effective approach for characterizing the dominant processes occurring within the cluster.

The internal kinetic energy of clusters exhibits fluctuations that tend to increase in proportion to the cluster size and the time since formation. This is the case both in the deviation from the time average of $\overline{\varepsilon_k}$ and in the standard deviation of the mean s_m for each data point. For example, in Fig. 2 we found $s_m(t_f = 100\text{ ps}) = 4.8$ meV, $s_m(t_f = 500\text{ ps}) = 7.7$ meV, and $s_m(t_f = 700\text{ ps}) = 12$ meV. This corresponds to the relative error increasing from ≈2%, to ≈7%, and to ≈17%. This effect is demonstrated in Figs. 2 and 4, where the ensemble average tends to broaden as time increases. This broadening is described by an increase of the s_m magnitude with the relaxation time. The relative magnitude of energy fluctuations generally becomes more significant in larger clusters.

There are two primary factors contributing to the observed fluctuations in the energy of clusters with larger sizes ($n = 5$ and above). The first factor is lower $\overline{\varepsilon_k}$ of the atoms in larger clusters compared with smaller clusters ($n \leqslant 4$). The second factor causing the time-dependent increase in fluctuations is purely statistical and arises from the depopulation of the ensemble of clusters with a given n due to nonequilibrium cluster growth $n \to n+1$. Fluctuations of the total cluster energy are relatively small compared with fluctuations of their kinetic energy.

Another notable feature can be seen in Figs. 3 and 5, which are the sharp short-term fluctuations in the total energy in the late stage of the relaxation. These fluctuations appear large in absolute values but have a relative magnitude of only ≈4%–5% from the surrounding smooth curves and look large due to the figure scales. These specific fluctuations do not exist in the kinetic energy time curves and arise due to fluctuation of the potential energy of clusters, i.e., fluctuations of their geometrical configurations. Some of these clusters present at the time of these sharp fluctuations have initial configurations far from equilibrium, which will have relaxation rates different from the average relaxation curve. Moreover, due to the reduction of the number of clusters in the ensemble with time since formation, the ensemble average becomes more sensitive to the contributions of clusters with initially highly excited potential energies.

We have compared the energies of a randomly chosen Ar atom and the single H^+ ion inside the Ar_nH^+ cluster. This was done by ensemble averaging the internal kinetic energies of individual Ar atoms bound inside an Ar_nH^+ cluster, without considering their specific locations within the cluster. We adopted this approach because we found that internal kinetic energies of the Ar atoms (regardless of location) inside the cluster are equivalent on average, although not shown. The ensemble-averaged internal kinetic energies for a cluster's single randomly chosen Ar, $\overline{\epsilon_{k,Ar}}$, and H^+, $\overline{\epsilon_{k,H^+}}$, particles have been inferred from the results of simulations for the entire relaxation process using the previously described methods. The results are shown for Ar_nH^+ clusters with $n = 4$ and 5 at $T = 40$ K in Figs. 6(a) and 6(b).

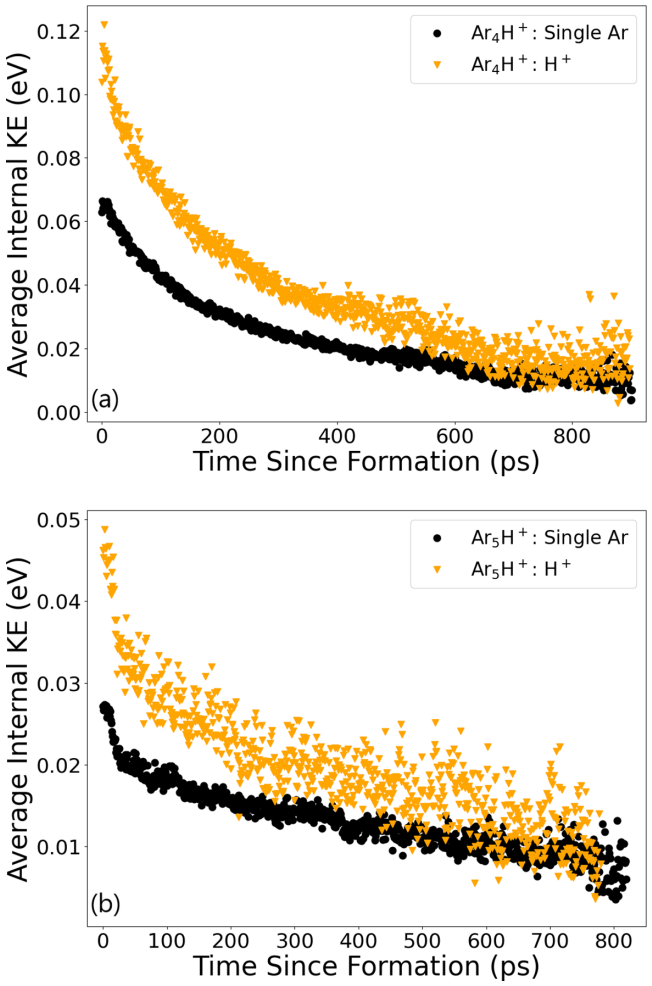

FIG. 6. Shown is $\overline{\epsilon_{k,Ar}}$ and $\overline{\epsilon_{k,H^+}}$ inside an (a) Ar_4H^+ and (b) Ar_5H^+ cluster. This average is calculated from the ensemble of simulations at $T = 40$ K. It is notable that the H^+ ion has ≈2 times the energy of a single Ar atom during the clusters' initial formation.

Several comments can be made based on these results. For the entire relaxation process in small Ar_nH^+ clusters, the H^+ ion has more kinetic energy than a single Ar atom. As the cluster size n increases, the difference in kinetic energies between the H^+ ions and Ar atoms decreases with n as it is shown in Figs. 6(a) and 6(b); this behavior between the H^+ and the cluster's Ar atoms was seen in other size clusters, $n = 3$, 6, 7, etc., although not shown. And once the cluster has reached $n = 8$, the internal kinetic energies of the single Ar and the H^+ become comparable. The difference in kinetic energies of the H^+ and Ar atoms is expected due to the general rule of the kinetics of energy relaxation: that light particles in a heavy bath gas (Lorentz gas) relax slower than heavy

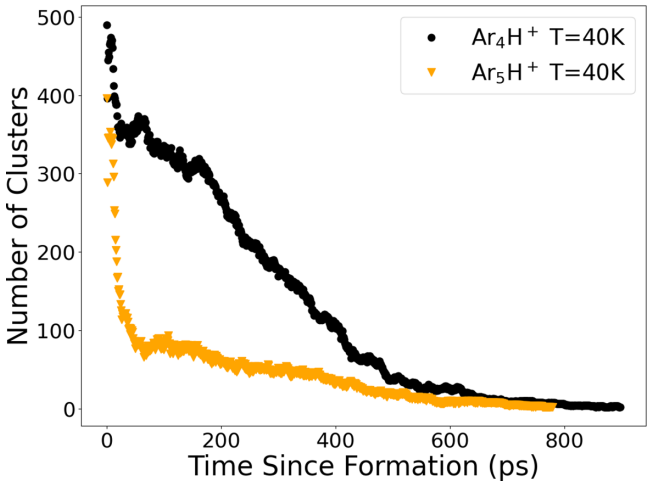

FIG. 7. Shown is the number of Ar_4H^+ (upper curve) and Ar_5H^+ (lower curve) clusters present in their respective ensembles since their time of formation. The number of clusters is inferred from the ensemble of simulations at $T = 40$ K. We see that the decrease is relatively smooth across all times since formation for the Ar_4H^+ clusters; for the Ar_5H^+ clusters there is a sharp decrease in the first ≈60 ps followed by relatively flat behavior and a smooth decrease.

particles in the same gas [44]. The mass ratio between the hot particle and bath gas particle impacts the rate of energy transfer during collisions. This mass difference explains the more pronounced fluctuations in the kinetic energy of the H^+ ions. Moreover, the energy fluctuations of the Ar atoms are smaller than compared with the H^+, due to the ensemble average for the single Ar having a factor of n more data points (since the average is calculated over all Ar atoms inside the Ar_nH^+ cluster).

VI. NONEQUILIBRIUM GROWTH AND LIFETIMES OF Ar_nH^+ CLUSTERS

In our simulation ensemble, we tracked the time-dependent velocities and coordinates of all particles inside the clusters of size n and also recorded the number $N(n,t)$ of such clusters as a function of the time since their formation. This allowed us to observe a notable behavior within the ensemble of growing nanoparticles, specifically the time-dependent growth and depletion of the number of the Ar_nH^+ clusters of the selected size n. The time dependencies of the number of clusters $N(n,t)$ with $n \leqslant 11$ have been inferred from the database on the nonequilibrium cluster growth in the ensemble of 500 independent clusters. To exemplify typical features of the time-evolution of the cluster population $N(n,t)$, we show the inferred number of Ar_4H^+ and Ar_5H^+ clusters as the functions of time since their formation in Fig. 7.

The depicted small fluctuations in the number of clusters reflect the stochastic nature of the nucleation process. Two types of behavior of the ensemble population $N(n,t)$ are observed. For very small clusters with $n \leqslant 4$, the depopulation curves $N(n,t)$ are relatively smooth, as illustrated in Fig. 7 for $n = 4$, until the majority of the clusters in the initial ensemble are cooled down and undergo a size change due to $n \to n+1$ transitions. The relatively fast but small initial drop of the $N(n,t)$ values, as it is shown in Fig. 7, can be explained by the small fraction of the metastable clusters decaying in $n \to n-1$ transitions and n-size growth of Ar_nH^+ clusters with highly excited configurations. The latter cluster can quickly leave the Ar_nH^+ ensemble due to efficient long-range sticking $n \to n+1$ or dissociative $n \to n-1$ collisions with the cold bath gas atoms.

In the Ar_nH^+ clusters with $n \leqslant 4$, all atoms belong to the first most stable and tight atomic shells [52]. The growth of Ar_nH^+ clusters, with $n \geqslant 5$, leads to the formation of the outer, loosely bound solvation shells. The presence of inner and outer atomic shells determines the distinct time-behavior of the nonequilibrium population $N(n,t)$. Simulations show a sharp decrease in the number of clusters in the Ar_nH^+ ($n \geqslant 5$) ensembles within the first ≈50–80 ps, followed by a slower decrease that takes much longer compared with the initial rapid decrease. An example of this general structure is shown in Fig. 7 for the nascent Ar_5H^+ clusters. Their depopulation is characterized by two distinct timescales: one that is fast, around 60 ps, and another that is much longer, approximately 700–800 ps. The rapid phase of depopulation coincides with a sharp drop (≈15%–20%) in the value of average internal kinetic energy, as shown in Fig. 6(b). This correlation will be discussed in the next section.

Under the conditions of nonequilibrium growth, the lifetime τ_n of Ar_nH^+ clusters can be defined as an ensemble-averaged time-interval required for the decay of the initial nonequilibrium population of Ar_nH^+ with the following steady growth of $Ar_{n+1}H^+$. The degradation of the cluster population $N(n,t)$ occurs in multiple $n \to n \pm 1$ transitions in cluster collisions with Ar atoms of the ambient gas. In our simulations, the nonequilibrium rate of cluster growth in $n \to n+1$ collisions is larger than the rate of the detachment processes $n \to n-1$. The smaller clusters with only inner atomic shell $n \leqslant 4$, have longer lifetimes compared with ones with $n \geqslant 5$. This behavior is completely consistent with the general statement that the probability of collisional capture of Ar atoms from the cold bath gas increases significantly with the reduction of the energy of cluster particles belonging to the outer cluster shells. The magnitude of the excitation on nascent clusters in the $n \to n+1$ process is sharply decreasing with n and becomes roughly constant for $n \geqslant 5$. This is a reflection of the n dependence of the binding energy of Ar atoms in the outer shells of Ar_nH^+ clusters.

Several collision processes contribute to the fast cluster growth and so to the depopulation of Ar_nH^+ ($n \geqslant 5$) ensembles of the nascent clusters with the outer shells of Ar atoms. The nascent Ar_nH^{+*} ($n \geqslant 5$) clusters are formed in highly excited states with a large variety of excited configurations provided by outer shell Ar atoms. These atoms significantly impact the rates of cluster energy relaxation and growth. The simplified model of cluster nucleation dynamics presented below is not exact, but it can be rationalized for clusters with $n \geqslant 5$, owing to the significant contrast in the binding energies of Ar atoms in the first and second atomic shells [52].

The configurations of the nascent excited Ar_nH^{+*} can be approximately classified into two groups: (a) long-range configurations and (b) short-range (tight) configurations. In the (a)-type configurations, incoming Ar atoms are captured in

the long-range but shallow attractive part of the potential of interaction between the $Ar_{n-1}H^+$ cluster core and the incoming free Ar atom. For example, for the excited Ar_5H^{+*}, the capture of a free Ar atom into the outer shell with the long-range configuration occurs mostly in Ar + Ar collisions of free atoms inside the long-range potential field of the Ar_4H^+ cluster core. This is a direct analogy to the three-body recombination processes in a dense plasma [13], where the cluster core plays the role of the "third" body. As these collisions occur within the shallow region of the potential well, both the kinetic and potential energies of the captured Ar atoms in the outer shell are comparatively low. The Ar atoms in the outer shell can efficiently exchange energies with the cold bath gas and, at the same time, participates in cooling the hot atoms of the cluster core. Notice that, for clusters with $n \geqslant 5$, both the cluster core and outer shell can be in excited states.

Then (b)-type (tight) configurations are mostly formed in direct sticking collisions between the cluster core and free Ar atoms. Here in the cluster core region, the kinetic energy of the incoming free Ar atom becomes large and can be transferred to the core particles, e.g., in an inelastic collision exciting internal rotational-vibrational states. This will cause the outer shell Ar atom to remain near the core region for the entire relaxation process, and the outer shell Ar atom in this "tight" configuration will have relatively large values of the internal kinetic energy. The (b)-type configurations are more close to the equilibrium ones more so than the long-range configurations (a). The energy relaxation of the (b)-type nascent Ar_5H^{+*} clusters looks similar to the slow relaxation of the strongly bound and tight Ar_4H^{+*}.

Our simulations were performed at the high density of the Ar bath gas (10^{20} cm^{-3}). For this very high density the rate of sticking collisions populating (a) configurations is higher than the rate of direct collisions with the cluster core creating the (b)-type clusters. The phase volume of the long-range (a) configurations is significantly larger than that of the tight configurations (b). Thus, we expect that the ensemble population of nascent Ar_nH^{+*} ($n \geqslant 5$) clusters with outer shells are mostly formed and decay due to the population of the (a)-type long-range configurations. Estimates for the Ar_5H^{+*} clusters, based on the analysis of simulation results and simplified modeling of $Ar_4H^+ + Ar$ potential, show that about 60%–70% of nascent Ar_5H^{+*} are formed with the long-range configurations (a).

There are a variety of collision processes in each configuration (a) and (b) that can lead to the significant and fast drop in cluster population in Fig. 7. For the (a)-type clusters with the outer shell atoms, all growth and relaxation processes are expected to be relatively fast, ∼50–80 ps, while the "tight" configurations provide the longer timescale of the $n \to n+1$ growth transitions.

The detailed analysis of any specific type of sticking (inelastic) collisions between free atoms and molecules or small clusters, such as $Ar_nH^+ + Ar \to Ar_{n+1}H^{+*}$, requires specific quantum-mechanical or semiclassical calculations [55–57], which are a part of our future projects. Nevertheless, we can describe a general feature of the sticking collision between clusters and bath gas atoms. In isolated nanosize systems with a finite value of the phase space, the small system is expected to return to its initial state after some finite amount of time τ_r. If this time is much longer than the time between collisions, the excited nascent cluster can reduce internal energy in these collisions and stabilize a size transition. Moreover, τ_r should increase with cluster size (more available degrees of freedom), which leads to an increase in cluster growth due to its ability to have many stabilizing collisions.

VII. COLLISIONAL COOLING OF NASCENT Ar_nH^+ CLUSTERS

Collisions between bath gas atoms and excited Ar_nH^{+*} clusters result in the relaxation of the internal energy of the nascent clusters and initiate their growth. Our MD simulations provide detailed information on the time-dependent relaxation of the cluster's internal energies. To analyze the simulation data on the cooling of small clusters we have used numerical solutions of the Boltzmann kinetic equation. Computational methods were developed in our previous study of the time-dependent energy relaxation of hot atoms in molecular and atomic gases [45–48].

The kinetic energies of individual particles belonging to the nascent clusters are significantly higher than thermal ones, and the energy relaxation of the cluster's particles in collisions with the cold Ar atoms can be described as cluster cooling. The computational scheme has been significantly simplified because the encounter between the cluster's Ar atoms and free Ar atoms is sufficiently rapid due to the short range of the Ar-Ar potential. Such encounters can be considered as a spatially localized "point" collision, resulting in an exchange in the particle's kinetic energies exclusively. Accurate rates of energy transfer, i.e., rates of cluster cooling, can be calculated using known differential cross sections of elastic and inelastic collisions of atomic or molecular particles [47,48]. For our purposes, the simplest hard-sphere approximation (HSA) has been utilized as the collision model for the short-range forces associated with Ar atoms [44,48]. Although the $H^+ + Ar$ potential includes a long-range tail arising from the Ar's polarization, the energy transfer in H^+ and Ar collisions can be also described by the HSA model with an appropriate transport cross section. We computed the time-dependent kinetic-energy distribution function for hot cluster particles using the Boltzmann equation:

$$\frac{\partial}{\partial t} f_n(\epsilon_k, t) = \int B(\epsilon_k|\epsilon'_k) f_n(\epsilon'_k, t) d\epsilon'_k - f_n(\epsilon_k, t) \times \int B(\epsilon'_k|\epsilon_k) d\epsilon'_k + Q_n(\epsilon_k, t), \quad (1)$$

where $f_n(\epsilon_k, t)$ is the kinetic-energy distribution function for the hot Ar or H^+ particles within an Ar_nH^+ cluster, $B(\epsilon_k|\epsilon'_k)$ is the energy relaxation kernel representing the rates of $\epsilon'_k \to \epsilon_k$ transitions due to collisions of cluster particles with the bath gas atoms, and $Q_n(\epsilon_k, T)$ is the sink or source function describing the production or removal of the Ar_nH^+ clusters with the specific kinetic energies ϵ_k of the cluster's particles. Under conditions of the strong nonequilibrium growth, the rate of $n \to n+1$ transitions dominates and this depopulates the initial nonequilibrium Ar_nH^+ ensemble. In the Appendix, we provide an analytical expression for the $B(\epsilon_k|\epsilon'_k)$ kernel and discuss details of the numerical solution of the Boltzmann equation.

In the framework of the relaxation-time approximation [13], the sink term $Q_n(\epsilon_k, t)$ in Eq. (1) can be expressed via the empirical lifetime $\tau_n(\epsilon_k)$ of Ar_nH^+ clusters:

$$Q_n(\epsilon_k, t) = -f_n(\epsilon_k, t)/\tau_n(\epsilon_k), \tag{2}$$

where $\tau_n(\epsilon_k)$ is the characteristic time describing the reduction of Ar_nH^{+*} cluster populations due to the $n \to n+1$ growth transitions and any weak evaporation processes. The relationship between the timescales of the cluster cooling and growing processes depends on the number of Ar atoms in the cluster n, which also defines the number of cluster atomic shells. All relaxation processes, including cluster growth and cooling, occur significantly faster in the clusters with outer shells, as it was discussed in Sec. VI.

The cluster cooling and the cluster growth both take place due to collisions with Ar bath gas atoms. In our simulations, we observed two main scenarios for the nonequilibrium cluster nucleation. The first scenario happens when the clusters cool down faster than they grow. The second scenario, on the other hand, manifests the opposite situation where the rate of cluster growth is faster than the rate of cooling of the internal degrees of freedom.

Scenario 1. *The relaxation of the cluster internal energy regulates cluster growth*. This "cooling and growth" scenario works for very small clusters with $n \leqslant 4$, where the equalization of energies of Ar atoms belonging to the deepest atomic shell occurs very quickly due to strong Ar-Ar and Ar-H^+ interactions at the relatively small distances between individual particles inside the clusters. Under such conditions, the cooling collisions with the bath gas atoms influence simultaneously all cluster particles. The energy relaxation rates for every Ar atom and their mean energy are about the same for the entire cooling process. Although the initial kinetic energy of the light H^+ is larger than the energy of heavy Ar atoms, as shown in Figs. 6(a) and 6(b), both relaxation processes are accomplished with the same cooling time due to efficient energy exchange between cluster particles. They are strongly correlated and their energy relaxation processes are well described by the Boltzmann equations.

The time-dependent energy distribution functions $f_n(\epsilon_k, t)$ for the hot Ar and H^+ particles inside nascent Ar_nH^+ clusters have been determined through the numerical solutions of the Boltzmann equation with the initial distribution function extracted directly from our ensemble of simulations. The obtained solutions of Eq. (1) were used for computations of the time-dependent average kinetic energies $\overline{\epsilon_{k,Ar}}$ of Ar and $\overline{\epsilon_{k,H^+}}$ of H^+ cluster particles. The results are in very good agreement with the data inferred from the simulations of the growth and cooling of small clusters with $n \leqslant 4$. In Figs. 8 and 9 we show the results for the MD simulations of the time-dependent energy relaxations of both Ar and H^+ particles within Ar_4H^+ nascent cluster in comparisons with the theoretical predictions, indicated by the solid curves. The theoretical curves shown in Fig. 8 or in Fig. 9 have been computed with a single fitting parameter, the effective hard-sphere cross section, σ: $\sigma_{Ar} = 1.5 \times 10^{-14}$ cm^2 for Ar + Ar collisions or $\sigma_{H^+} = 2.4 \times 10^{-14}$ cm^2 for Ar+H^+ collisions. These parametric cross sections are in general agreement with the quantum cross sections computed for collisions of free particles [58,59]. In the numerical calculations of the kinetic-energy relaxation of Ar_nH^+ ($n \leqslant 4$) clusters, $Q_n(\epsilon_k, t)$ can be ignored because the lifetime of these clusters is mostly determined by their cooling rates.

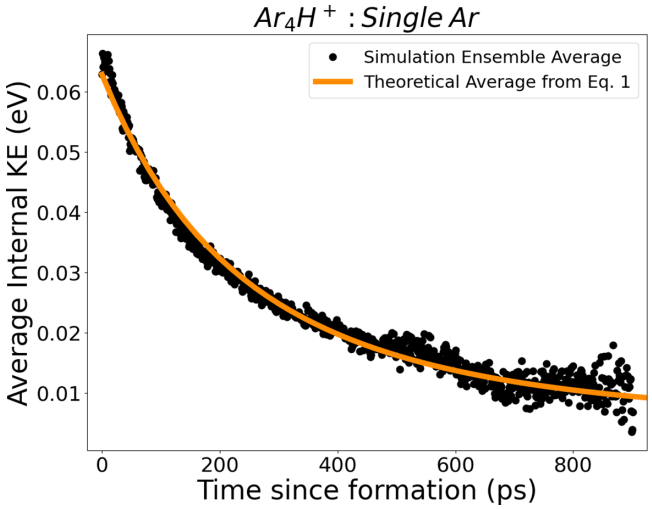

FIG. 8. Shown is $\overline{\epsilon_{k,\mathrm{Ar}}}$ inside an Ar_4H^+ cluster, from the ensemble of $T = 40$ K simulations, alongside the theoretical time-dependent average calculated from the Boltzmann equation using the initial distribution function found directly from our ensemble of simulations as the initial distribution.

The excellent agreement between the theoretical predictions and results of simulations indicates that the growth of ultrasmall clusters ($n \leqslant 4$) with the open or closed first atomic shell occurs mostly as the internal kinetic energy of cluster particles has been cooled enough to increase the Ar sticking probability in $Ar_nH^+ + Ar$ collisions.

Scenario 2. *The fast growth of larger clusters: effect of outer cluster shells*. The processes of internal energy relaxation and cluster growth can be substantially altered if the rate of cluster growth surpasses that of cluster cooling. This phenomenon

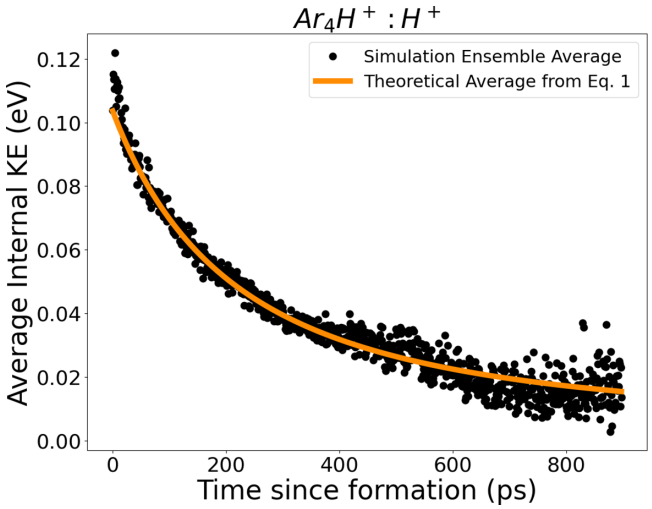

FIG. 9. Shown is $\overline{\epsilon_{k,H^+}}$ inside an Ar_4H^+ cluster, from the ensemble of $T = 40$ K simulations, alongside the theoretical time-dependent average calculated from the Boltzmann equation using the initial distribution function found directly from our ensemble of simulations as the initial distribution.

manifests in sufficiently large Ar_nH^+ clusters, wherein the interactions of outer or inner cluster shells with the surrounding bath gas atoms differ. Ar atoms in the outer shells have significantly smaller binding energies, and this creates favorable conditions for the redistribution of kinetic energy from the incoming Ar atoms over various internal degrees of freedom and increasing the probability of $n \to n+1$ sticking collisions. The fast dynamics of the energy relaxation and growth of the clusters with outer shells ($n \geqslant 5$), i.e., shorter lifetime of Ar_nH^+ clusters, are correlated with the presence of their long-range configurations (a) as it was discussed in Sec. VI. The different relaxation rates of the long-range (a) and tight (b) configurations affect the time dependence of the average kinetic energy computed using the Boltzmann equation, and thus should not be neglected.

To include the distinction between the cooling of inner and other cluster shells, the distribution function $f_n(\epsilon_k, t)$ in Eq. (1) is formally split into two independent distribution functions $f_n(\epsilon_k, t) = w_a * f_{n,a}(\epsilon_k, t) + w_b * f_{n,b}(\epsilon_k, t)$, one for the long-range (a) and tight (b) configurations discussed in Sec.VI. The statistical weight w_a and w_b describe the initial populations of the long-range and tight configurations ($w_a + w_b = 1$). The decay rates of the cluster populations with the (a) long-range or (b) tight configurations, i.e., the different dynamics of the cluster growth for each configuration, are given by the independent sink functions $Q_{n,a}$ and $Q_{n,b}$:

$$Q_{n,i} = -f_{n,i}(\epsilon_k, t)/\tau_{n,i}(\epsilon_k), \quad i = a, b, \tag{3}$$

where $\tau_{n,a}$ and $\tau_{n,b}$ are the lifetimes for the cluster with the long-range and tight configurations respectively. Details of the computation procedure for these distribution functions are given in the Appendix.

The cluster growth in $n \to n+1$ transitions requires a few collisions between Ar_nH^{+*} ($n \geqslant 5$) and free Ar atoms. Such collisions mostly involve clusters with the (a)-type (long-range) configurations, which are predominately populated (w_a significantly exceeds w_b). Complete decay of the long-range population occurs for the short time ≈50–70 ps. It involves a larger fraction of the Ar_nH^{+*} ensemble ($w_a > 60\%$) but does not strongly influence the averaged kinetic energies of the cluster Ar ($\overline{\epsilon_{k,Ar}}$) and H^+ ($\overline{\epsilon_{k,H^+}}$) particles. The energy-relaxation of the small fraction of the nascent clusters with the (b)-configuration is similar to the relatively slow relaxation of Ar_nH^{+*} ($n \leqslant 4$), except for highly excited metastable configurations. The empirical values for the lifetime parameters $\tau_{n,a}$ and $\tau_{n,b}$ for different configurations allow a very good agreement between theoretical predictions of the dynamics of the cluster cooling and results of the simulations. To illustrate the dynamics of the cooling clusters with inner and outer shells, we show in Figs. 10 and 11 the results of the MD simulations and theoretical analysis of the energy relaxation of Ar ($\overline{\epsilon_{k,Ar}}$) and H^+ ($\overline{\epsilon_{k,H^+}}$) particles in Ar_5H^+ clusters.

The parameters required for the theoretical description of the Ar_5H^+ cluster cooling and growth processes via solutions of the Boltzmann equation are determined for Ar and H^+ cluster particles. For the Ar atom's cooling the following parameters were extracted: $\sigma_{Ar} = 1.3 \times 10^{-14}$ cm^2, $\tau_{a,Ar} =$ 23 ps. The energy dependent lifetime of the (b)-type clusters reflects the decay of the clusters with high kinetic energies

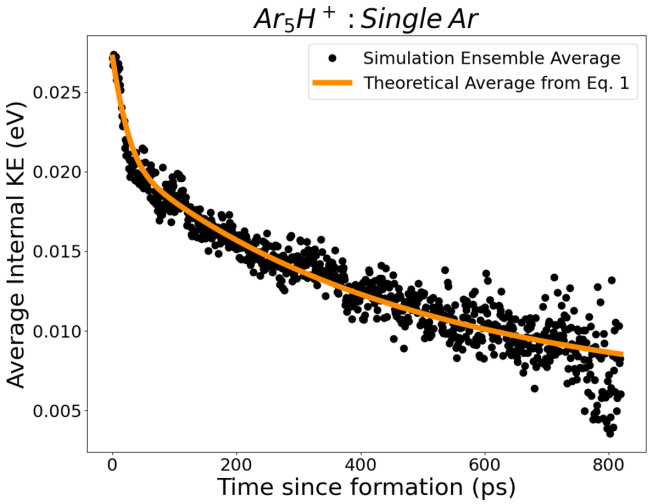

FIG. 10. Shown is $\overline{\epsilon_{k,Ar}}$ inside an Ar_5H^+ cluster, from the ensemble of $T = 40$ K simulations, alongside the time-dependent average calculated from the Boltzmann equation with the presence of $Q_n(\epsilon_k, t)$, and using the initial distribution function directly from our ensemble of simulations to initialize the (a) and (b) initial distributions.

and is given by $\tau_b(\epsilon_k) = \tau_b\{1 + \exp[-(\epsilon_k - \epsilon_c)/\epsilon_w]\}$. In the expression for $\tau_{b,\mathrm{Ar}}$ the scaling time is $\tau_b = 15$ ps and the energy parameter, $\epsilon_c = 59$ meV, corresponding to the kinetic-energy threshold above which the tight populations of clusters quickly decays and ϵ_w describing the energy width of this threshold region. In our numerical calculations, the width of the threshold areas was simply taken as $0.2k_BT$, as it is described in the Appendix. The computational parameters for the energy relaxation of H^+ are $\sigma_{H^+} = 2.8 \times 10^{-14}$ cm^2, $\tau_{a,H^+} = 17$ ps, $\tau_{b,H^+} = 11$ ps, and $\epsilon_{c,H^+} = 100$ meV. The statistical weights of the long-range and tight configurations are $w_a \simeq 63\%$ and $w_b \simeq 37\%$ respectively. The proposed

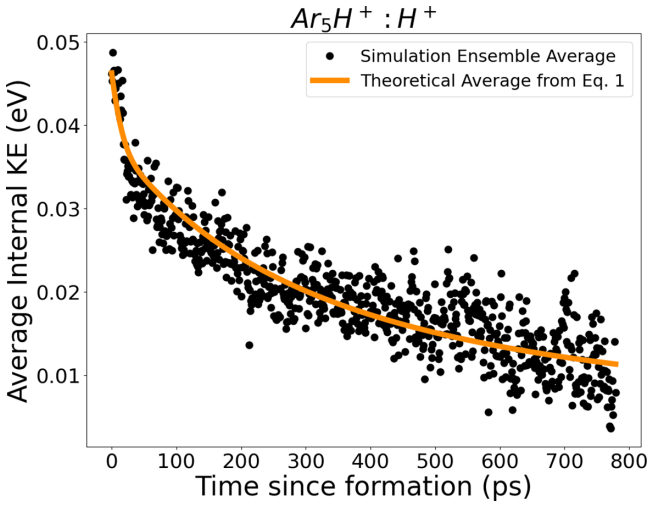

FIG. 11. Shown is $\overline{\epsilon_{k,H^+}}$ inside an Ar_5H^+ cluster, from the ensemble of $T = 40$ K simulations, alongside the time-dependent average calculated from the Boltzmann equation with the presence of $Q_n(\epsilon_k, t)$, using the initial distribution function directly from our ensemble of simulations to initialize the (a) and (b) initial distributions.

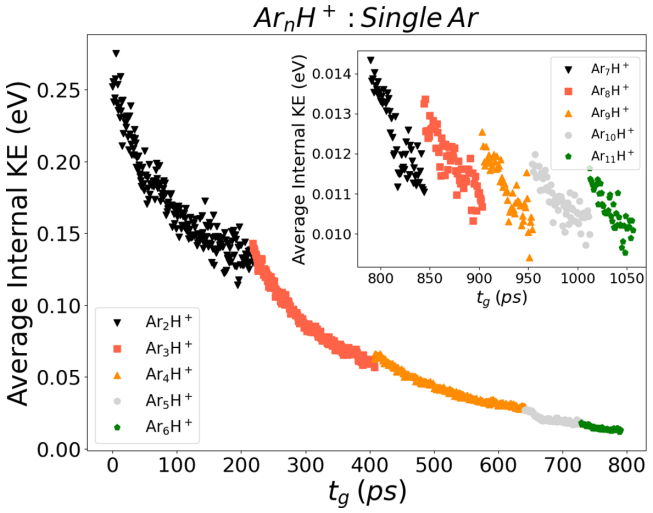

FIG. 12. Shown is $\overline{\epsilon_{k,Ar}}$ inside an average $Ar_{n(t_g)}H^+$ cluster, starting from $n = 2$, from the ensemble of $T = 40$ K simulations. The different markers and colors represent different n, increasing from left to right across the figure ($n = 2$ to $n = 6$). The inset shows the range of $n = 7$ to $n = 11$.

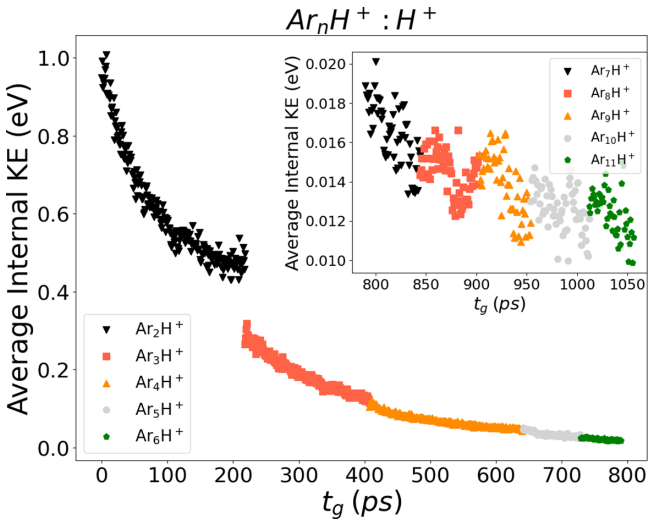

FIG. 13. Shown is $\overline{\epsilon_{k,H^+}}$ inside an average $Ar_{n(t_g)}H^+$ cluster, starting from $n = 2$, from the ensemble of $T = 40$ K simulations. The different markers and colors represent different n, increasing from left to right across the figure ($n = 2$ to $n = 6$). The inset shows the range of $n = 7$ to $n = 11$.

theoretical model recreates the sharp depopulation of the nascent Ar_5H^{+*} clusters in the first ≈50–80 ps as it is shown in Fig. 7 and accurately describes the cluster cooling processes depicted in Figs. 10 and 11.

VIII. Ar OR H^+ PARTICLES IN A SINGLE PERMANENTLY GROWING CLUSTER

In previous sections, we described the relaxation dynamics in the ensemble of small clusters with specified sizes n. An alternative approach is to analyze the parameters of Ar and H^+ cluster particles in a single permanently growing cluster as regular particles representing an embryo of a new phase. In this view, the Ar_nH^+ cluster, independently of their value of n, can be treated as an open subsystem that exchanges energy and particles with the bath Ar gas [52]. Thus, it is possible to randomly sample a single Ar atom or H^+ ion from the cluster phase at any time during the nonequilibrium cluster growth. Such sampling allows us to establish an averaged behavior of particles inside the new phase, i.e., the growth of a single $Ar_{n(t_g)}H^+$ cluster with an increasing number of Ar atoms $n(t_g)$, where t_g is the time since the beginning of the growth process. To model the averaged time evolution of the particle inside the growing embryo of new phase, we can use the averaged kinetic energies, $\overline{\epsilon_{k,Ar}}$ and $\overline{\epsilon_{k,H^+}}$, inferred from the simulation ensembles of Ar_nH^+ clusters with the specific n values. We are suggesting, that the growing cluster gains particles after the average lifetime, estimated in our simulations, for the specific size n. According to this approach, the averaged kinetic energies $\overline{\epsilon_{k,Ar}}$ and $\overline{\epsilon_{k,H^+}}$ in a growing cluster are represented by data shown in Figs. 12 and 13, respectively.

There are few general trends in the data shown for the Ar and H^+ particles. When a cluster undergoes a nonthermal size transitions, $n \to n + 1$, there may be a discontinuity in $\overline{\epsilon_{k,Ar}}$ and $\overline{\epsilon_{k,H^+}}$ values. This is expected for small clusters because capturing free Ar atom(s) leads to the sharp excitation of the internal degrees of freedom in the cluster. These jumps in the kinetic energies typically decrease with increasing cluster size. A related discontinuity was also observed in the total internal kinetic energy of individual clusters, ε_k, as shown in Fig. 1. These discontinuities vanished when clusters reached equilibrium with the ambient Ar gas (equilibration of the chemical potential of two phases). At this equilibrium stage, the energy of thermal fluctuations became comparable with values of energy jumps at $n \to n \pm 1$ transitions.

The data presented in Fig. 13 indicates a notable reduction in the average H^+ kinetic energy during the cluster growth process from the $n = 2$ to $n = 3$ state. Specifically, the observed decrease in kinetic energy can be explained by the efficient loss of the H^+ kinetic energy due to interaction with an additional Ar in the inner atomic shell. Processes of cooling and excitation of the cluster's H^+ ion are significantly transformed with the growth of the cluster size. In ultrasmall clusters as well as small molecular ions, the ion can lose kinetic energy due to permanent efficient encounters with the heavy Ar atoms from the inner shell and also due to long-range interactions with free Ar atoms from the bath gas. In terms of molecular physics, these collisions can efficiently quench highly excited rovibrational modes involving the motion of the H^+ ion [56,57]. For the large-size clusters with inner and outer atomic shells, where the H^+ is trapped inside the Ar cage, the direct energy transfer collisions between H^+ and free Ar are less effective, and cooling of all cluster particles occurs mostly due to Ar + Ar collision involving the bath gas.

The data in Figs. 12 and 13 show the general cooling of the internal energy of the new phase (clusters) during the nonequilibrium stage of the cluster growth. The randomly chosen Ar atom and H^+ cluster particles in the ensemble of independently growing clusters represent the relaxation dynamics of the new phase. Growth and cooling processes are compensated when the new phase reached equilibrium at $T =$ 40 K, and fluctuations of the cluster size and particle energies

are described by the thermodynamic equilibrium between two phases, the free Ar gas and the Ar cluster atoms [52].

IX. CONCLUSION

We conducted MD simulations to study nucleation and nonequilibrium growth of nanoparticles; focusing on three fundamental aspects of small cluster nucleation: (1) the formation of nascent nanoclusters with highly excited kinetic and configurational (potential) energies, (2) the competition between cluster growth and internal energy relaxation, and (3) the influence of the cluster shell structures and parameters of the ambient gas on the cluster cooling and growth rates. Our conclusions were based on the data from simulations of Ar_nH^+ cluster nucleation initiated by a H^+ ion in the cold metastable Ar gas and theoretical modeling of time-dependent relaxation processes. Our findings show that at low temperatures ($T = 40$ K) small nascent clusters with $n \leqslant 11$ are created in the states with high values of kinetic energy and with configurations that are far from equilibrium. Such type of excited states of the new phase is a common feature of the recombination and relaxation phenomena in plasma and atomic physics [13].

Collisions of the cluster particles with the Ar bath gas atoms are responsible for both cooling and growing processes. Both processes can strongly influence each other, and for the nanosize Ar_nH^+ clusters, the resulting rates of cooling and growth depend on the cluster shell structure, cluster size, temperature, and density of the ambient gas. As the Ar_nH^+ cluster grows, the scale of excitation of nascent clusters decreases with increasing n, and the growth process becomes more diffusive in nature.

It was also observed that within the small Ar_nH^+ ($n \leqslant 4$) clusters, the kinetic energies of inner shell Ar atoms are quickly equalized on timescales much shorter than the typical collisional time between the cluster and the bath gas atoms. The tight configurations of these very small clusters and large kinetic energies of the inner particles require significant time to cool the cluster's internal degrees of freedom; and to provide the necessary conditions for cluster growth, such as an increase in the probability of sticking collisions of the bath gas atoms with the cluster.

The Ar_nH^+ ($n \geqslant 5$) clusters, with inner and outer atomic shells, demonstrate different dynamics for their energy relaxation and growth. Small kinetic and potential energies of the outer shell Ar atoms in the long-range cluster configurations, and their efficient interaction with the cold bath gas yield a significant increase in the cluster growth rate, which becomes larger than the rates of corresponding cooling collisions.

The results of the MD simulations of the cluster cooling and growth can be described by a simplified model of cluster energy relaxation due to short-range energy-transfer collisions between hot cluster particles and cool Ar atoms of the ambient gas. It was shown in the framework of a simple model, the numerical solutions of the Boltzmann equation for the energy relaxation of hot Ar and H^+ cluster particles in the cold Ar gas are in very good agreement with the results of simulations for clusters with the inner Ar shell ($n \leqslant 4$). Theoretical description of the time-dependent energy relaxation and growth of Ar_nH^+ ($n \geqslant 5$) clusters also provides a good agreement with the result of MD simulations, but it requires the use of empirical formulas for the rate of growth for clusters with outer atomic shells.

The data on the cooling of the ensemble of Ar_nH^+ clusters with specific number n of Ar atoms have been used to illustrate the averaged energy relaxation processes in the permanently growing cluster with the time-increasing number of atoms $n = n(t_g)$.

The results of the present work provide a deep insight into the characteristics and intensity of relaxations processes responsible for the nucleation and growth of nanosize clusters in a cold atomic gas in the presence of ionized particles.

ACKNOWLEDGMENTS

V.K. acknowledges support from the National Science Foundation through Grant No. PHY-2116679 for the ITAMP at the Harvard- Smithsonian Center for Astrophysics; R.C. was supported by the National Science Foundation, Grant No. PHY-2034284.

APPENDIX

The cooling of the internal energy of nascent clusters predominately occurs in short-range binary collisions of the free Ar atoms with individual cluster particles. These short-time and short-range encounters are mostly responsible for changes in the kinetic energies of colliding particles and can be considered as elemental steps of the internal energy relaxation of nascent Ar_nH^+ clusters. The rate of the kinetic-energy-transfer process $\epsilon'_k \to \epsilon_k$ in short-range collisions between the hot cluster particles and Ar atoms of the bath gas can be described by the kernel of the Boltzmann kinetic equation $B(\epsilon_k|\epsilon'_k)$ expressed via the anisotropic differential cross sections [47,48]. Relatively expansive numerical calculations are required to establish $B(\epsilon_k|\epsilon'_k)$'s functional form, but significant simplification in the solution of the Boltzmann equation can be achieved if the energy and angular dependence of the cross sections are neglected [44,48]. This replacement of real cross sections with the hard sphere provides rather accurate description of the time evolution of energy distribution functions of hot particles in atomic and molecular collisions. The values of a single empirical parameter of the hard-sphere approximation, the cross section σ, are usually close to values of corresponding momentum-transfer cross sections.

To efficiently solve Eq. (1), we transform it into a unitless equation, where unitless energy e is measured in multiples of k_BT, with k_B as the Boltzmann constant, $e = \epsilon_k/k_BT$. The unitless time is given by $\tau = n_b\sigma v_T t$ where n_b is the density of the bath gas, σ is the HSA cross section, $v_T = \sqrt{2k_BT/m}$ is the scaling thermal velocity, and m is the mass of the hot cluster particle which is the Ar or H^+. Unitless kinetic energies of the cluster particles before and after a single collision are

$$e_{\rm in} \equiv \frac{\epsilon_{k,\rm in}}{k_BT}, \quad e_{\rm out} \equiv \frac{\epsilon_{k,\rm out}}{k_BT}. \tag{A1}$$

The ratio of the hot particle mass m to the mass m_b of Ar bath gas atoms, $\kappa = m/m_b$, is a fundamental parameter of the energy relaxation kinetics [44] regulating the rate of momentum or energy transfer in the binary collisions.

The unitless kernel of the Boltzmann equation $b(e_{\rm out}|e_{\rm in})$ can be written as [44,48]

$$b(e_{\rm out}|e_{\rm in}) = \frac{(\kappa+1)^2}{8\kappa\sqrt{e_{\rm in}}} \times \begin{cases} e^{(e_{\rm in}-e_{\rm out})}\left[\mathrm{erf}\left(\frac{(\kappa+1)\sqrt{e_{\rm in}}+(\kappa-1)\sqrt{e_{\rm out}}}{2\sqrt{\kappa}}\right) - \mathrm{erf}\left(\frac{(\kappa+1)\sqrt{e_{\rm in}}-(\kappa-1)\sqrt{e_{\rm out}}}{2\sqrt{\kappa}}\right)\right] \\ +\mathrm{erf}\left(\frac{(\kappa-1)\sqrt{e_{\rm in}}+(\kappa+1)\sqrt{e_{\rm out}}}{2\sqrt{\kappa}}\right) - \mathrm{erf}\left(\frac{(\kappa-1)\sqrt{e_{\rm in}}-(\kappa+1)\sqrt{e_{\rm out}}}{2\sqrt{\kappa}}\right) \\ \text{if } e_{\rm in} > e_{\rm out} \\ \mathrm{erf}\left(\frac{(\kappa-1)\sqrt{e_{\rm in}}+(\kappa+1)\sqrt{e_{\rm out}}}{2\sqrt{\kappa}}\right) - \mathrm{erf}\left(\frac{-(\kappa-1)\sqrt{e_{\rm in}}+(\kappa+1)\sqrt{e_{\rm out}}}{2\sqrt{\kappa}}\right) \\ +e^{(e_{\rm in}-e_{\rm out})}\left[\mathrm{erf}\left(\frac{(\kappa+1)\sqrt{e_{\rm in}}+(\kappa-1)\sqrt{e_{\rm out}}}{2\sqrt{\kappa}}\right) - \mathrm{erf}\left(\frac{-(\kappa+1)\sqrt{e_{\rm in}}+(\kappa-1)\sqrt{e_{\rm out}}}{2\sqrt{\kappa}}\right)\right] \\ \text{if } e_{\rm in} < e_{\rm out}. \end{cases} \tag{A2}$$

where $\mathrm{erf}(x)$ is the error function. This transforms Eq. (1) into the following:

$$\frac{\partial}{\partial\tau} f(e,\tau) = \int b(e|e')f(e',\tau)de' - f(e,\tau)\int b(e'|e)de'. \tag{A3}$$

The sink or source term $Q(e,\tau)$ does not influence the cooling rates of Ar_nH^{+*} clusters with $n \leqslant 4$ and it is omitted in Eq. (A3) for simplicity.

For the numerical solution of Eq. (A3), the energy of the hot particle is discretized with N small steps δe, where $\delta e \ll 1$. In our solution, the unitless energies e and e' have been discretized with the bin width $\delta e = 0.01$, i.e., the discrete step in calculations of the real kinetic energies was $0.01k_BT$. The small value of δe has been selected to verify an accurate convergence of numerical solutions of Eq. (A3) to the Maxwell distribution as $\tau \to \infty$. The number of bins N can be different for the clusters of different sizes n. The discrete kinetic-energy distribution functions of the Ar and H^+ particles of the nascent clusters were directly inferred from the results of simulations. These distributions have been used as the initial distribution functions in solutions of Eq. (A3).

In the discrete representation, the kinetic-energy distribution functions of hot cluster particles $f(e,\tau)$ are given by the N-dimensional vector $\vec{\mathrm{f}}(\tau)$. The kernel of the discretized kinetic equation is represented by the tensor $\mathbf{W}_{ij}$, the $N \times N$ matrix. Shown are the formal discretizations of energy, $\vec{\mathrm{f}}(\tau)$, and Eq. (A3):

$$\begin{aligned} \vec{\mathrm{e}} &= \left[\frac{\delta e}{2}, \frac{3\delta e}{2}, \frac{5\delta e}{2}, \ldots, e_{\max} - \frac{\delta e}{2}\right], \quad \delta e = \frac{e_{\max}}{N}, \\ \vec{\mathrm{f}}(\tau) &= [f(e_1,\tau),\ f(e_2,\tau),\ \ldots,\ f(e_N,\tau)], \\ w_{ij} &= b(e_i|e_j)\delta e, \\ \frac{d}{d\tau}f_i &= \sum_{j=1}^{N} w_{ij}f_j - f_i\sum_{j=1}^{N} w_{ji} \\ &= \sum_{j=1}^{N}\left(w_{ij} - \delta_{ij}\sum_{j=1}^{N} w_{ji}\right)f_j \\ &= \sum_{j=1}^{N} W_{ij}f_j, \\ \frac{d}{d\tau}\vec{\mathbf{f}} &= \mathbf{W}\vec{\mathbf{f}}, \quad \mathbf{W}_{ij} \equiv w_{ij} - \delta_{ij}\sum_{j=1}^{N} w_{ji}. \end{aligned} \tag{A4}$$

The formal solution of Eq. (A4) for the vector $\vec{\mathbf{f}}(\tau)$ was obtained using the evolution operator $\exp[\tau\mathbf{W}]$ [60,61]:

$$\vec{\mathrm{f}}(\tau) = \exp[\tau\mathbf{W}]\tilde{\mathbf{f}}(0), \tag{A5}$$

where $\mathbf{f}(0)$ [45] is the initial energy distribution function. The computed vector functions $\vec{\mathrm{f}}(\tau)$ have been converted back to the distribution function $f_n(\epsilon_k,t)$ of the kinetic energies of hot particles within Ar_nH^+ clusters, as written in Eq. (1).

The obtained time-dependent distribution functions $f_n(\epsilon_k,t)$ have been employed for calculations of the time-dependent averaged energy $\langle\epsilon_{k,n}(t)\rangle$ of the Ar_nH^{+*} ($n \leqslant 4$) cluster particles:

$$\overline{\epsilon_{k,n}} = \int f_n(\epsilon_k,t)\epsilon_k d\epsilon_k, \tag{A6}$$

The results of these calculations were used for the analysis of cooling and growing processes in nanoclusters with $n \leqslant 4$ as shown in Figs. 8 and 9 for Ar and H^+ cluster particles.

The significant difference in the cluster growth (Fig. 7) and cooling processes (Figs. 8 and 10) can be seen for clusters with the inner $n \leqslant 4$ and outer $n \geqslant 5$ shells. Computation of the time-dependent energy distribution functions of hot particles inside rapidly growing clusters with the outer atomic shell(s) requires a consideration of the decay of the nascent Ar_nH^{+*} ($n \geqslant 5$) population due to relatively fast $n \to n \pm 1$ transitions. Thus, the presence of the sink function, $Q_n(\epsilon_k,t)$, cannot be ignored in the numerical analysis of the cooling processes for clusters with $n \geqslant 5$.

The configurations of the nascent Ar_nH^+ excited clusters can be formally split into two categories described in Sec. VI: (a) the long-range configurations with low kinetic and potential energies of the outer shell Ar atoms interacting effectively with the Ar bath gas; and (b) the tight configurations where outer shell Ar atoms with significant kinetic energies are trapped close to the inner shell. These configurations are characterized by the different relaxation processes and time-dependent distribution functions $f_{n,a}(\epsilon_k,t)$ and $f_{n,b}(\epsilon_k,t)$. The statistical weights w_a and w_b ($w_a + w_b = 1$) of these configurations in the ensemble of nascent Ar_nH^+ cluster can be inferred from the results of simulations, but in the present modeling, w_a has been employed as the fitting parameter. For example, we evaluated from the fitting of the simulation results that $w_a \simeq 0.63$ and $w_b \simeq 0.37$ for the ensemble of nascent Ar_5H^{+*} clusters. The sink function for the $f_{n,i}(\epsilon_k,t)$ distributions ($i = a, b$) can be written as $Q_{n,i} = -f_{n,i}(\epsilon_k,t)/\tau_{n,i}(\epsilon_k)$, where $\tau_{n,i}(\epsilon_k)$ are the scaling lifetime for the clusters with the long-range or tight configurations.

The population of the (a)-type of Ar_nH^{+*} clusters with long-range configurations and relatively small kinetic energies decays very quickly due to $n \rightarrow n+1$ growth transitions involving collisions between the outer shell Ar atoms and cold atoms of the bath gas. These transitions occur very quickly and the dependence of the lifetime $\tau_{n,a}(\epsilon_k)$ from the kinetic energies of outer shell Ar atoms can be neglected: $\tau_{n,a}(\epsilon_k) \simeq \tau_{n,a}$.

The lifetime of the clusters with the tight configurations (b) can depend on the kinetic energies of the cluster particles. Although the potential energies, i.e., configurations of the (b)-type clusters, are close to the equilibrium values of Ar_nH^+, these excited clusters have been created with the relatively high kinetic energies in the direct collisions between free Ar atoms and the cluster core, the cluster particles from the inner shell. The relaxation processes for the (b)-type tight configurations are similar to the relaxation of the tight clusters with inner shell only ($n \leqslant 4$). The lifetime $\tau_{n,b}(\epsilon_k)$ can be relatively long because of the high kinetic energies of cluster particles and relatively slow cooling processes. On the other hand, the presence of highly energetic cluster particles with kinetic energies above some threshold $\epsilon_{c,n}$ can lead to redistribution of the internal kinetic energy inside the cluster and following detachments of the weakly bound Ar atoms from the outer shells, i.e., decay of the Ar_nH^{+*} cluster population. We have used an empirical expression for the lifetime of the clusters with the tight (b) configurations, which describe the discussed above lifetime behavior:

$$\tau_b(\epsilon_k) = \tau_b\{1 + \exp\left[-(\epsilon_k - \epsilon_{c,n})/\epsilon_w\right]\}, \tag{A7}$$

where $\epsilon_{c,n}$ is the empirical kinetic-energy threshold for the stability of clusters with the outer shells, τ_b is the empirical scaling time, and ϵ_w describes the energy width of the threshold region, which was taken as $0.2k_BT$. This value was chosen such that $1/\tau_b(\epsilon_k)$ will act similarly to a step function with narrow width around the threshold energy. The last equation shows that the energy dependent lifetime of the high energy fraction of $f_{n,b}(\epsilon_k, t)$ is relatively short, but for the bulk of the $f_{n,b}(\epsilon_k, t)$ distribution the decay process is slower than the typical time required for the energy relaxation. The relaxation of these long-living configurations was shown similar to the relaxation of Ar_nH^+ ($n \leqslant 4$) clusters, and therefore their decay can also be neglected in solving the Boltzmann kinetic equation.

[1] W. M. Grundy, T. Bertrand, R. Binzel, M. Buie, B. Buratti, A. Cheng, J. Cook, D. Cruikshank, S. Devins, C. Dalle Ore, A. Earle, K. Ennico, F. Forget, P. Gao, G. Gladstone, C. Howett, D. Jennings, J. Kammer, T. Lauer, I. Linscott *et al.*, Icarus **314**, 232 (2018).

[2] A. Wellbrock, A. J. Coates, G. H. Jones, V. Vuitton, P. Lavvas, R. T. Desai, and J. H. Waite, Mon. Not. R. Astron. Soc. **490**, 2254 (2019).

[3] P. Gao, D. P. Thorngren, E. K. H. Lee, J. J. Fortney, C. V. Morley, H. R. Wakeford, D. K. Powell, K. B. Stevenson, and X. Zhang, Nat. Astron. **4**, 951 (2020).

[4] A. D. James, J. S. A. Brooke, T. P. Mangan, T. F. Whale, J. M. C. Plane, and B. J. Murray, Atmos. Chem. Phys. **18**, 4519 (2018).

[5] A. V. Egorov, E. N. Brodskaya, and A. Laaksonen, Colloid J. **80**, 484 (2018).

[6] X. Yang and A. W. Castleman, Jr., J. Geophys. Res. **96**, 22573 (1991).

[7] A. V. Krivov, I. Mann, and N. A. Krivova, Astron. Astrophys. **362**, 1127 (2000).

[8] A. V. Krivov, T. Löhne, and M. Sremčević, Astron. Astrophys. **455**, 509 (2006).

[9] I. Mann, Philos. Trans. R. Soc., A **375**, 20160254 (2017).

[10] J. W. Schmelzer, J. Non-Cryst. Solids **356**, 2901 (2010).

[11] E. Cloet, *ASM Handbook, Fundamentals of Modeling for Metals Processing* (ASM International, 2009), Vol. 22, pp. 203–219.

[12] S. Karthika, T. K. Radhakrishnan, and P. Kalaichelvi, Cryst. Growth Des. **16**, 6663 (2016).

[13] E. M. Lifshitz and L. Pitaevskii, *Physical Kinetics* (IOP Publishing, Ltd., Oxford, UK, 2010).

[14] V. V. Hoang and T. Odagaki, Phys. Rev. B **77**, 125434 (2008).

[15] R. S. Dumont, S. Jain, and A. G. Basile, J. Chem. Phys. **102**, 4227 (1995).

[16] C. Rey, L. Gallego, M. Iñiguez, and J. Alonso, Phys. B (Amsterdam, Neth.) **179**, 273 (1992).

[17] K. Laasonen, S. Wonczak, R. Strey, and A. Laaksonen, J. Chem. Phys. **113**, 9741 (2000).

[18] T. Kraska, J. Chem. Phys. **124**, 054507 (2006).

[19] O. C. F. Brown, D. Vrinceanu, V. Kharchenko, and H. R. Sadeghpour, Mol. Phys. **118**, e1767813 (2020).

[20] A. Sepehri, S. Amjad-Iranagh, K. Golzar, and H. Modarress, Chem. Phys. **423**, 135 (2013).

[21] W. Xu, Z. Lan, B. L. Peng, R. F. Wen, and X. H. Ma, J. Chem. Phys. **142**, 054701 (2015).

[22] A. Pérez and A. Rubio, J. Chem. Phys. **135**, 244505 (2011).

[23] E. Brodskaya, A. P. Lyubartsev, and A. Laaksonen, J. Chem. Phys. **116**, 7879 (2002).

[24] K. S. Karadima, V. G. Mavrantzas, and S. N. Pandis, Phys. Chem. Chem. Phys. **19**, 16681 (2017).

[25] M. Gatchell, P. Martini, L. Kranabetter, B. Rasul, and P. Scheier, Phys. Rev. A **98**, 022519 (2018).

[26] D. C. McDonald, D. T. Mauney, D. Leicht, J. H. Marks, J. A. Tan, J.-L. Kuo, and M. A. Duncan, J. Chem. Phys. **145**, 231101 (2016).

[27] K. T. Giju, S. Roszak, and J. Leszczynski, J. Chem. Phys. **117**, 4803 (2002).

[28] J. A. Tan and J.-L. Kuo, J. Phys. Chem. A **124**, 7726 (2020).

[29] K. Vafayi and K. Esfarjani, J. Cluster Sci. **26**, 473 (2015).

[30] H. Schöbel, P. Bartl, C. Leidlmair, S. Denifl, O. Echt, T. D. Märk, and P. Scheier, Eur. Phys. J. D **63**, 209 (2011).

[31] T. Kurzthaler, B. Rasul, M. Kuhn, A. Lindinger, P. Scheier, and A. M. Ellis, J. Chem. Phys. **145**, 064305 (2016).

[32] M. Kuhn, M. Renzler, J. Postler, S. Ralser, S. Spieler, M. Simpson, H. Linnartz, A. G. G. M. Tielens, J. Cami, A. Mauracher, Y. Wang, M. Alcamí, F. Martín, M. K. Beyer, R. Wester, A. Lindinger, and P. Scheier, Nat. Commun. **7**, 13550 (2016).

[33] P. W. Stephens and J. G. King, Phys. Rev. Lett. **51**, 1538 (1983).

[34] H. Buchenau, E. L. Knuth, J. Northby, J. P. Toennies, and C. Winkler, J. Chem. Phys. **92**, 6875 (1990).
[35] I. A. Harris, R. S. Kidwell, and J. A. Northby, Phys. Rev. Lett. **53**, 2390 (1984).
[36] I. Harris, K. Norman, R. Mulkern, and J. Northby, Chem. Phys. Lett. **130**, 316 (1986).
[37] T. D. Märk and P. Scheier, Chem. Phys. Lett. **137**, 245 (1987).
[38] M. Lezius, P. Scheier, A. Stamatovic, and T. D. Märk, J. Chem. Phys. **91**, 3240 (1989).
[39] W. Miehle, O. Kandler, T. Leisner, and O. Echt, J. Chem. Phys. **91**, 5940 (1989).
[40] M. Gatchell, P. Martini, A. Schiller, and P. Scheier, J. Am. Soc. Mass Spectrom. **30**, 2632 (2019).
[41] A. E. Korenchenko, A. G. Vorontsov, and B. R. Gel'chinskii, High Temp. **54**, 229 (2016).
[42] P. Kolorenč, V. Averbukh, R. Feifel, and J. Eland, J. Phys. B: At., Mol. Opt. Phys. **49**, 082001 (2016).
[43] M. A. Miller, J. P. K. Doye, and D. J. Wales, Phys. Rev. E **60**, 3701 (1999).
[44] K. Andersen and K. E. Shuler, J. Chem. Phys. **40**, 633 (1964).
[45] P. Zhang, V. Kharchenko, M. J. Jamieson, and A. Dalgarno, J. Geophys. Res. **114**, A07101 (2009).
[46] N. Balakrishnan, E. Sergueeva, V. Kharchenko, and A. Dalgarno, J. Geophys. Res. **105**, 18549 (2000).
[47] S. Bovino, P. Zhang, V. Kharchenko, and A. Dalgarno, J. Chem. Phys. **135**, 024304 (2011).
[48] V. Kharchenko, N. Balakrishnan, and A. Dalgarno, J. Atmos. Sol.-Terr. Phys. **60**, 95 (1998).
[49] I. Napari and H. Vehkamäki, J. Chem. Phys. **124**, 024303 (2006).
[50] I. Napari and H. Vehkamäki, J. Chem. Phys. **125**, 094313 (2006).
[51] A. P. Thompson, H. M. Aktulga, R. Berger, D. S. Bolintineanu, W. M. Brown, P. S. Crozier, P. J. in 't Veld, A. Kohlmeyer, S. G. Moore, T. D. Nguyen, R. Shan, M. J. Stevens, J. Tranchida, C. Trott, and S. J. Plimpton, Comput. Phys. Commun. **271**, 108171 (2022).
[52] M. G. Rozman, M. Bredice, J. Smucker, H. R. Sadeghpour, D. Vrinceanu, R. Côté, and V. Kharchenko, Phys. Rev. A **105**, 022807 (2022).
[53] J. Wedekind, D. Reguera, and R. Strey, J. Chem. Phys. **127**, 064501 (2007).
[54] T. Ritschel, C. Zuhrt, L. Zülicke, and P. J. Kuntz, Eur. Phys. J. D **41**, 127 (2007).
[55] R. C. Forrey, V. Kharchenko, N. Balakrishnan, and A. Dalgarno, Phys. Rev. A **59**, 2146 (1999).
[56] T. Stoecklin, P. Halvick, M. A. Gannouni, M. Hochlaf, S. Kotochigova, and E. R. Hudson, Nat. Commun. **7**, 11234 (2016).
[57] A. K. Hansen, O. O. Versolato, Ł. Kłosowski, S. B. Kristensen, A. Gingell, M. Schwarz, A. Windberger, J. Ullrich, J. R. C. López-Urrutia, and M. Drewsen, Nature (London) **508**, 76 (2014).
[58] A. V. Phelps, C. H. Greene, J. P. Burke, Jr., and A. V. Phelps, J. Phys. B: At., Mol. Opt. Phys. **33**, 2965 (2000).
[59] A. V. Phelps, J. Phys. Chem. Ref. Data **21**, 883 (1992).
[60] C. Moler and C. Loan, Soc. Ind. Appl. Math. **45**, 3 (2003).
[61] N. J. Higham, SIAM J. Matrix Anal. Appl. **26**, 1179 (2005).